Brain Research Bulletin 190 (2022) 234–243

Contents lists available at ScienceDirect

Brain Research Bulletin

journal homepage: www.elsevier.com/locate/brainresbull

Super-resolution imaging and quantitative analysis of microtubule arrays in model neurons show that epothilone D increases the density but decreases the length and straightness of microtubules in axon-like processes☆

Christian Conze[a,1], Nataliya I. Trushina[a,1], Michael Holtmannspötter[b], Marina Rierola[a], Simone Attanasio[a], Lidia Bakota[a], Jacob Piehler[b,c], Roland Brandt[a,b,d,*]

[a] Department of Neurobiology, Osnabrück University, Osnabrück, Germany
[b] Center for Cellular Nanoanalytics, Osnabrück University, Osnabrück, Germany
[c] Division of Biophysics, Osnabrück University, Osnabrück, Germany
[d] Institute of Cognitive Science, Osnabrück University, Osnabrück, Germany

ARTICLE INFO

Keywords:
Neuronal microtubules
Tubulin dynamics
Single-molecule localization microscopy (SMLM)
Point Accumulation in Nanoscale Topography (PAINT)
Microtubule targeting drugs
Epothilone

ABSTRACT

Microtubules are essential for the development of neurons and the regulation of their structural plasticity. Microtubules also provide the structural basis for the long-distance transport of cargo. Various factors influence the organization and dynamics of neuronal microtubules, and disturbance of microtubule regulation is thought to play a central role in neurodegenerative diseases. However, imaging and quantitative assessment of the microtubule organization in the densely packed neuronal processes is challenging. The development of super-resolution techniques combined with the use of nanobodies offers new possibilities to visualize microtubules in neurites in high resolution. In combination with recently developed computational analysis tools, this allows automated quantification of neuronal microtubule organization with high precision. Here we have implemented three-dimensional DNA-PAINT (Point Accumulation in Nanoscale Topography), a single-molecule localization microscopy (SMLM) technique, which allows us to acquire 3D arrays of the microtubule lattice in axons of model neurons (neuronally differentiated PC12 cells) and dendrites of primary neurons. For the quantitative analysis of the microtubule organization, we used the open-source software package SMLM image filament extractor (SIFNE). We found that treatment with nanomolar concentrations of the microtubule-targeting drug epothilone D (EpoD) increased microtubule density in axon-like processes of model neurons and shifted the microtubule length distribution to shorter ones, with a mean microtubule length of 2.39 μm (without EpoD) and 1.98 μm (with EpoD). We also observed a significant decrease in microtubule straightness after EpoD treatment. The changes in microtubule density were consistent with live-cell imaging measurements of ensemble microtubule dynamics using a previously established Fluorescence Decay After Photoactivation (FDAP) assay. For comparison, we determined the organization of the microtubule array in dendrites of primary hippocampal neurons. We observed that dendritic microtubules have a very similar length distribution and straightness compared to microtubules in axon-like processes of a neuronal cell line. Our data show that super-resolution imaging of microtubules followed by algorithm-based image analysis represents a powerful tool to quantitatively assess changes in microtubule organization in neuronal processes, useful to determine the effect of microtubule-modulating conditions. We also provide evidence that the approach is robust and can be applied to neuronal cell lines or primary neurons, both after incorporation of labeled tubulin and by anti-tubulin antibody staining.

☆ For the Special Issue „Cytoskeletal Proteins in Health and Neurodegenerative Disease: Concepts and Methods“, *Brain Research Bulletin*

* Correspondence to: Department of Neurobiology, Osnabrück University, Barbarastraße 11, D-49076 Osnabrück, Germany.
E-mail address: robrandt@uni-osnabrueck.de (R. Brandt).

[1] These Authors contributed equally.

https://doi.org/10.1016/j.brainresbull.2022.10.008
Received 18 July 2022; Received in revised form 3 October 2022; Accepted 6 October 2022
Available online 13 October 2022

1. Introduction

Neurons are the main unit of the nervous system and are required for the transmission and processing of information provided by electrical or chemical signals. This requires a complex structural organization and dynamic remodeling to adapt to changes in the environment during the lifetime of an organism. Neurons are highly polarized cells with a single axon that extends from the cell body to some considerable length and transmits signals, and several shorter dendrites, which receive signals.

Along with actin filaments, the microtubule cytoskeleton is fundamental to establish and maintain the morphology and function of neurons. Individual microtubules are long and straight hollow cylinders composed of α- and β-tubulin heterodimers that attach head-to-tail to protofilaments that associate into tubular structures about 25 nm in diameter (Kapitein and Hoogenraad, 2015; Penazzi et al., 2016a). In neurites, microtubules are aligned in longitudinal parallel bundles that run along the axon and dendrites, often accompanied by neuronal intermediate filaments (neurofilaments). While neurofilaments are known to regulate the diameter of axons and are particularly abundant in large-caliber vertebrate axons, the structural backbone of neurons appears to be the array of microtubules that maintain their specialized morphologies and functions (Prokop, 2020). In addition, microtubules serve as a long-distance railway system for the active transport of proteins, organelles, mRNAs, and cytoskeletal elements in axons and dendrites (Maday et al., 2014). The microtubule array extends from the soma to the tips of axons and dendrites, but individual microtubules do not span the entire length. While some microtubules are less than a micron in length, others can reach 100 μm or even more. The dimensions of neuronal microtubule length vary with organisms and cell type, but at least in developing mammalian axons and dendrites, average microtubules are only a few micrometers long (Bray and Bunge, 1981; Chalfie and Thomson, 1979; Joshi et al., 1986; Letourneau, 1982; Nishida et al., 2020; Okabe and Hirokawa, 1988; Weiss and Mayr, 1971; Yogev et al., 2016; Yu and Baas, 1994). The functionality of microtubules is regulated by various factors such as microtubule-associated proteins (MAPs) such as tau, MAP2, or MAP6, which bind to the microtubule polymer and regulate their dynamics and stability in a compartment-specific manner (Baas et al., 2016; Brandt et al., 2020). Furthermore, plus-end tracking proteins (+TIPs) can promote microtubule polymerization through dynamic accumulation at growing microtubule ends (Akhmanova and Steinmetz, 2015). Other proteins such as stathmin sequester soluble tubulin dimers and shift the microtubule population toward disassembly. Microtubule-severing enzymes, namely katanin, spastin, and fidgetin, cause microtubule fragmentation (McNally and Roll-Mecak, 2018). In addition, metabolic changes such as redox and calcium homeostasis can modulate microtubule dynamics and stability properties (Tian et al., 2020; Wilson and Gonzalez-Billault, 2015).

Critical events during neurodegenerative conditions and diseases are changes in microtubule regulation, dynamics, and organization that affect vital microtubule-dependent processes such as transport (Brandt and Bakota, 2017; Dubey et al., 2015; Millecamps and Julien, 2013). The microtubule organization in terms of polymer lengths, microtubule number, the spatial distribution of individual microtubules as well as the axial distribution of cytoskeletal intersections contribute to the efficiency and regulation of neuronal transport in an interplay with other factors such as post-translational modifications (PTMs) or interactions with MAPs (Balint et al., 2013; Conze et al., 2022).

The association of microtubule breakdown observed in neurodegeneration creates a desire to directly visualize the microtubule array in high resolution to improve our understanding of the sequence of events during neurodegeneration. In addition, sensitive methods to analyze changes in the neuronal microtubule array would be of great use for the identification and characterization of potential drugs that interfere with microtubule structure and dynamics. Such microtubule-targeting agents (MTAs), which include the epothilones that have been shown to cross the blood-brain barrier and have the potential to modulate neuronal microtubule dynamics and stability, may have the potential to restore disrupted microtubule-dependent processes during neurodegeneration (Ruschel et al., 2015; Soliman et al., 2022). However, the small diameter of neuronal processes and the densely packed microtubule organization make the visualization and quantitative assessment of changes in microtubule organization very challenging. To date, the gold standard for analyzing axonal or dendritic microtubule organization is the very labor-intensive serial section electron microscopy. The development of nanobodies during the last decade and their application in fluorescence-based super-resolution microscopy techniques offers new opportunities to visualize neuronal microtubule structure and organization in unprecedented ways (Mikhaylova et al., 2015). Combined with the application of computational strategies to analyze and quantify microtubule networks imaged by super-resolution microscopy, this approach paves the way to directly study changes in microtubule organization in neurons.

Here we implemented three-dimensional DNA-PAINT (Point Accumulation in Nanoscale Topography) (Jungmann et al., 2010), a single-molecule localization microscopy (SMLM) technique, which enabled us to acquire high-resolution images of the microtubule array in axon-like processes of model neurons and dendrites of primary neurons. For the quantitative analysis of microtubule distribution, we used the open-source software package SMLM image filament extractor (SIFNE) (Zhang et al., 2017). To validate the method, we determined the MTA epothilone D (EpoD) effect on the array of microtubules in axon-like processes at concentrations leading to increased microtubule polymerization. For comparison, we also determined the microtubule organization in the dendrites of primary hippocampal neurons. We report that the approach makes it possible to sensitively and quantitatively determine changes in microtubule length and density in axon-like processes mediated by MTAs. We show that microtubule organization is very similar in axon-like processes of model neurons and dendrites of cultured primary neurons. We also provide evidence that the approach is robust and can be applied to neuronal cell lines or primary neurons, both after incorporation of labeled tubulin and by anti-tubulin antibody staining.

2. Materials and methods

2.1. Materials

Chemicals, cell culture media, supplements, and plastic material were obtained from Sarstedt (Nümbrecht, Germany), Sigma-Aldrich (Deisenhofen, Germany), and Thermo-Fisher Scientific (Waltham, USA), unless otherwise stated. The microtubule-targeting agent epothilone D (EpoD) was a kind gift from Amos Smith 3rd (University of Pennsylvania) and was prepared as previously described (Lee et al., 2001; Rivkin et al., 2004). The purity of the compound was > 95 %, as determined by LC-MS and NMR analyses. The spectroscopic properties were identical to those reported in the literature.

2.2. Methods

2.2.1. Animals

C57BL/6J mice (Envigo, Netherlands) were used at embryonic stage 16–18 in order to generate low-density hippocampal primary cultures. All animals were kept and killed in accordance with the Ethical Committee on Animal Care and Use regulations of Lower Saxony, Germany.

2.2.2. Cell culture and transfection

PC12 cells, used as model neurons, were cultured in serum-DMEM as previously described (Fath et al., 2002). Transfections of PC12 cells were carried out with Lipofectamine 2000 (Thermo-Fisher Scientific, USA) as previously published (Fath et al., 2002). The expression plasmid for paGFP-α-Tubulin was created and used for Fluorescence Decay After Photoactivation (FDAP) experiments, as explained earlier (Janning

et al., 2014). The expression plasmid for mEGFP-α-Tubulin used for DNA-PAINT in PC12 cells was created as described earlier (Janning et al., 2014). For EpoD treatment, cells were incubated with 10 nM EpoD or vehicle control (0.01 % DMSO) for 1 h prior to imaging or fixation. For the cultivation of isolated hippocampal neurons, low-density hippocampal primary cultures were prepared as described previously (Fath et al., 2009). Briefly, hippocampi and cortices were separately dissected from mouse embryos on ice-cold phenol-red free Hank's Balanced Salt Solution (Thermo-Fisher Scientific, USA). Cells were mechanically dissociated and centrifuged at 100g for 15 min at 4 ºC. Approximately 10,000 hippocampal cells and a spatially separated high-dense rim of cortical neurons (approx. 250,000) were cultured in glass coverslip dishes (MatTek, USA) previously coated with poly-L-lysine and laminin. The culture medium of choice was Neurobasal-A (Thermo-Fisher Scientific, USA) supplemented with 2 % B27 (Thermo-Fisher Scientific, USA), 1 % glutamine 200 mM, and 0.5 % Pen-Strep. Cultured dishes were maintained at 37 ºC and 5 % CO_2 for 6–8 days in vitro (DIV) before further usage.

2.2.3. Live-cell imaging for photoactivation experiments

For Fluorescence Decay After Photoactivation (FDAP) experiments, PC12 cells were plated on poly-L-lysine and collagen-coated 35-mm glass-bottom culture dishes (MatTek, USA). 7 h after transfection, the medium was exchanged for DMEM with 1 % (vol/vol) serum without phenol red containing 100 ng/mL 7 S mouse NGF (Alomone Laboratories, Germany), thereby inducing neuronal differentiation. PC12 cell cultivation was continued for 4 days, and the culture medium was exchanged for serum-reduced DMEM containing NGF and without phenol red the day before live imaging. Photoactivation experiments were performed using a laser scanning microscope (Nikon Eclipse Ti2-E (Nikon, Japan) equipped with an LU-N4 laser unit with 488-nm and 405-nm lasers and a Fluor 60 × ultraviolet-corrected objective lens (NA 1.4)). The setup was enclosed in an incubation chamber, maintaining 37 °C and 5 % CO_2, preserving cell viability during microscopy. Automated image acquisition of paGFP-α-Tubulin expressing PC12 cells after photoactivation was essentially performed as published (Igaev et al., 2014). Briefly, a 6 μm long segment in the middle of a neurite was photoactivated with the 405-nm laser. Subsequently, a consecutive image series (time stack) was obtained at a frequency of 1 frame/s, while 112 frames were collected per activated cell at a resolution of 256 × 256 pixels.

2.2.4. FDAP data analysis

A reaction-diffusion model was used as described previously (Igaev et al., 2014) to estimate the average association rate k^*_{on} and the dissociation rate k_{off} constant of tubulin binding onto microtubules. Processing and analysis of individual FDAP curves were performed as previously described (Niewidok et al., 2016) using a custom-made C-based tool called cFDAP. The fitting procedure was used to obtain k^*_{on} and k_{off} from every single FDAP curve, while the $\chi 2$ value was used as an indicator of the goodness of fit of the model function.

2.2.5. Fixation and immunostaining

PC12 cells or primary neurons were treated with a combined NP-40 permeabilization-fixation protocol that removes membranes and cytosolic components but preserves cytoskeletal structures and associated proteins (Brandt et al., 1995; Lee and Rook, 1992). Briefly, cells were washed with PBS prior to permeabilization-fixation in presence of 0.5% (vol/vol) NP-40 % and 0.3 % (vol/vol) glutaraldehyde. Fixed cells were washed with PBS, incubated with 10 mg/mL $NaBH_4$, washed again, and incubated with 0.1 M glycine. Cells were finally washed with a BSA-PBS-Tween20 solution. The mEGFP-α-Tubulin tagged microtubule cytoskeleton of PC12 cells was immunostained using an anti-GFP nanobody obtained from the Massive-Tag-Q anti-GFP DNA-PAINT kit (Massive Photonics GmbH, Gräfelfing, Germany) diluted 1:100 (50 nM) in antibody-staining solution from the same kit and incubated overnight. The mEGFP-α-Tubulin tag in PC12 cells was used to enable the identification of transfected PC12 cells suitable for DNA-PAINT by epifluorescence microscopy prior to DNA-PAINT acquisition. For primary neurons, immunostaining was performed with a monoclonal anti--β-tubulin antibody (1:250, 480011; Invitrogen, USA) and anti-mouse Alexa Fluor® 488 (1:1000, A28175; Invitrogen, USA) as secondary antibody in order to visualize and select proper neurons to be imaged with DNA-PAINT. For DNA-PAINT of the same cells, microtubules were first detected with a polyclonal anti-α-tubulin antibody (PA5–19489; Invitrogen, USA) diluted 1:500 in BSA-PBS-Tween20 solution overnight at 4 °C. Subsequently, cells were washed with PBS, followed by the application of an oligonucleotide labeled anti-rabbit nanobody from the Massive-SDAB 1-PLEX kit (Massive Photonics GmbH, Gräfelfing, Germany) with a dilution of 1:100 (50 nM) in antibody staining solution from the same kit. Incubation was performed overnight at 4 °C. Cells were kept in PBS until imaging was performed.

2.2.6. Super-resolution microscopy with DNA-PAINT

For DNA-PAINT, cells were incubated with a 1:1000 dilution of 50 nm gold nanorods (Nanopartz, E12–50–600–25) as fiducial markers for 5 min at RT. Afterwards, samples were washed three times with PBS, after which 3 mL of imaging buffer (Massive Photonics) supplemented with 250 pM of Cy3b conjugated imager DNA-strand were added. For the visualization of the microtubule array in PC12 cells, the imager strand from the Massive-Tag-Q Anti-GFP DNA-PAINT kit was used, while for the visualization of the microtubule array in primary neurons, the imager from the rabbit-specific Massive-SDAB 1-PLEX kit was used. Cells were imaged with a total internal reflection fluorescence microscope (TIRFM) in the highly inclined and laminated optical sheet (HILO) mode (Tokunaga et al., 2008) using an inverted microscope frame (Olympus IX-81) equipped with a motorized quad-line TIR illumination condenser (cellTIRF-4-Line, Olympus) and a motorized xy-stage (Märzhäuser Scan IM 120 × 80). Three-dimensional single-molecule localization was achieved by astigmatic imaging using a cylindrical lens (Olympus) implemented directly in front of the filter wheel. To identify transfected PC12 cells or sufficiently labeled primary neurons suitable for DNA-Paint, excitation of GFP or Alexa Fluor® 488 was achieved by a 488 nm diode-pumped solid-state laser (max. power 150 mW, Olympus) while imager strands were excited with a 561 nm diode-pumped solid-state laser (max. power 150 mW, Olympus). Excitation light passed through a 100× oil immersion objective (UAPON 100× TIRF, NA 1.49, Olympus). For the excitation of imager strands, laser intensities were typically adjusted to 20–30 W/cm^2. Fluorescence emission was filtered by bandpass filters (BrightLine HC 525/50 for GFP and Alexa Fluor® 488 and BrightLine HC 600/37 for CY3b imager strands, Semrock) before being recorded with an sCMOS camera (ORCAFlash 4.0 V3, Hamamatsu). CellSens 2.2 (Olympus) was used as an acquisition software to record 80,000 frames with an exposure time of 150 ms per frame and a 2 × 2 pixel binning, which resulted in a pixel size of 130 nm. During acquisition, the sample focus plane was stabilized with a hardware autofocus system (IX2-ZDC2, Olympus). The temperature was kept stable at 25 °C, controlled by a large incubator chamber (TempController 2000–2, Pecon), while the sample was humidified via a small stage top incubator (CO_2-Controller 2000, Pecon) to exclude buffer evaporation. Axial calibration of astigmatic PSFs necessary for three-dimensional single-molecule localization microscopy was achieved by acquiring z-stacks of immobilized fluorescent TetraSpeck™ microspheres with a diameter of 100 nm (Invitrogen, T7279) at the beginning of an imaging session. Stacks were recorded in an imaging buffer with a step size of 10 nm using a piezo z-stage (NanoScanZ, NZ100, Prior Scientific).

2.2.7. Post-processing

Raw data sets were processed with the "Picasso" software package (Schnitzbauer et al., 2017) (https://github.com/jungmannlab/picasso). First, the calibration z-stack of TetraSpeck™ beads was analyzed with

"Picasso localize". For single bead identification, the box size was set to 13 and the Min. Net. Gradient was adjusted to filter out weak signals from unwanted background localizations. Photon conversion parameters were set as follows: EM Gain: 1, Baseline: 400, Sensitivity 0.46, Quantum Efficiency: 0.80 and pixel size: 130 nm. A calibration file was generated with the "Calibrate 3D" function of "Picasso localize". This file, as well as the same photon conversion parameters, were used for the image procession of raw sample files. The Min. Net. Gradient was adjusted to remove unspecifically bound imager strands or other background signal and thus filter for localizations with the highest signal intensities. Single-molecule localizations were fitted with a least-square Gaussian fit. For 3D localization, the magnification factor was set to 1.0. Processed datasets were opened with "Picasso render" and a drift correction was first conducted with cross-correlation, followed by a correction with gold nanorods as fiducials if enough fiducials were present in the acquired ROI. The localizations of the data sets were then exported for the ImageJ plugin ThunderSTORM for 3D rendering in order to obtain image-stacks with a well-defined voxel size set to (26 nm × 26 nm × 25 nm) based on the overall axial resolution of 25 nm (Ovesny et al., 2014).

2.2.8. SIFNE analysis

The computational analysis and quantification of the microtubule array in axon-like processes of PC12 cells and dendrites of primary neurons were performed by employing the open-source software package SIFNE (single-molecule localization microscopy image filament network extractor (Zhang et al., 2017). The MATLAB-based tool involves the iterative extraction of the filamentous structures from the image data set and the subsequent identification and assignment of the detected filaments. Although three-dimensional datasets with a depth between 600 and 800 nm were acquired, we had to create Maximum Intensity Projections (MIPs) from our datasets, as Zhang et al. developed their tool for 2D datasets only. Given that the axial spacing between microtubules in PC12 neurites is 70 ± 20 nm and 64 ± 10 nm in dendrites (Chen et al., 1992; Jacobs and Stevens, 1986), we chose optical sections with a thickness of 150 nm in PC12 cells and 100 nm in primary neurons for filament extraction by SIFNE. This allowed us to use sections where the resolution was highest while avoiding overlapping superimposed microtubules from another layer that would skew our statistics. The region of interest (ROI) was defined to be at least 10 μm in length in the axon shaft and separated from the initial segment of the axon and the growth cone. In dendrites of primary neurons, the ROI was set to unbranched dendritic segments of at least 8 μm in length. For image enhancement using line and orientation filter transform (LFT and OFT) algorithms, a radius of 10 pixels with 40 rotations of the scanning line segment was used. Segmentation was performed by employing the automatic threshold functionality of SIFNE based on Otsu's method. For creating a pool of minimal linear filament fragments, regions of filament intersections were removed by a local region around each intersection of 2 × 2 pixels. For recovering undetected linear structures, a 2-times iterative extraction of filaments was performed, followed by registration of the propagation direction of each filament tip. Grouping and analysis of detected filaments were performed using a pixel size of 26 nm and a maximum curvature of 1 rad/μm. Search angle and radius were set to 60° and 40 pixels, respectively. The allowable orientation difference between endpoints was set to 60°. The maximum allowable angle difference and endpoint gap vector were set to 60° and 30°, respectively. Weights for similarity and continuity conditions during scoring calculations were set to 1. Due to the high complexity of the cytoskeletal network, no fragment overlap was allowed, as suggested by (Zhang et al., 2017) for an intricate network. For sorting of composite filaments, the minimum filament length was set to 15 pixels corresponding to 390 nm, while ungrouped filaments were left in the dataset. As microtubules are accompanied by neuronal intermediate filaments (neurofilaments) that are known to regulate the diameter of axons, we referred our quantified parameters for microtubule density and mass to the length analyzed region and not to the diameter or area.

3. Results

3.1. The microtubule-targeting agent epothilone D (EpoD) increases the amount of microtubule polymer in axon-like processes

To identify conditions leading to microtubule polymer alteration in neurites, we employed a previously established quantitative live cell imaging assay and the well-characterized microtubule-targeting agent (MTA) epothilone D (EpoD). This small-molecule microtubule stabilizer binds to the β-tubulin subunit on the luminal surface of microtubules, induces tubulin polymerization similar to paclitaxel (Buey et al., 2004), and reduces spine loss in an Alzheimer's disease model already at a subnanomolar concentration (Penazzi et al., 2016b). We used a Fluorescence Decay After Photoactivation (FDAP) approach after incorporation of photoactivatable GFP (paGFP)-tagged tubulin (paGFP-α-Tubulin) into the neuronal microtubule array. A population of the tagged tubulin was focally activated in the middle of axon-like processes, and the FDAP was monitored over time in the region of activation (Fig. 1A, B). Treatment with 10 nM EpoD decreased the FDAP compared to the carrier-control, indicating the microtubule-stabilizing activity of the MTA (Fig. 1C). To determine the fraction of free and bound tubulin, we fitted the FDAP curves with a reaction-diffusion model (Janning et al., 2014). The amount of polymerized tubulin was increased by ~8 % after treatment with EpoD, associated with a trend towards an increased average k_{on} rate constant and a significant decrease in k_{off} (Fig. 1D, E). Thus, the data show that treatment with nanomolar concentrations of the MTA EpoD induces an increase in microtubule polymer in axon-like processes of model neurons.

3.2. Super-resolution imaging of microtubule arrays in axon-like processes

We used super-resolution microscopy with DNA-PAINT to analyze the microtubule array of neuronal processes at high resolution. The basic idea of PAINT (Points Accumulation for Imaging in Nanoscale Topography) is that the structure of interest is labeled with freely diffusing dyes or dye-labeled ligands that transiently bind to the molecules of interest. The PAINT concept is superior to other SMLM techniques because it is easy to implement, does not require complex experimental conditions to enable fluorophore photoswitching, and offers theoretically unlimited imaging cycles due to the transient nature of the dye-binding mechanism. In combination with DNA nanotechnology, it is possible to use a tunable target-probe interaction system with high specificity. Typically, a system of two complementary DNA oligomers between 7 and 10 nucleotides in length is used. The so-called docking strand is conjugated to an antibody or nanobody that targets a protein of interest, while the complementary dye-conjugated imager DNA strand freely diffuses inside the imaging buffer (Agasti et al., 2017). This imager is only detectable upon interaction with the docking strand, allowing the collection of a large number of photons from a single position and thus enabling very high localization precision (Schnitzbauer et al., 2017).

To visualize the microtubule lattice in axon-like processes of model neurons using super-resolution microscopy with DNA-PAINT, we imaged differentiated PC12 cells transfected with mEGFP-α-Tubulin using total internal reflection fluorescence (TIRF) microscopy in the highly inclined and laminated optical sheet (HILO) mode, which allows an imaging depth of up to 10 μm (Tokunaga et al., 2008). To enable a direct comparison with the FDAP's live cell imaging approach, we chose to express exogenous α-tubulin with a construct under the same promoter. The approach utilized the transient hybridization between oligonucleotide strands tagged to nanobodies against GFP and free diffusing dye-labeled (Cy3B) oligonucleotide strands. This enables single-molecule localization with nanometer resolution, laterally below

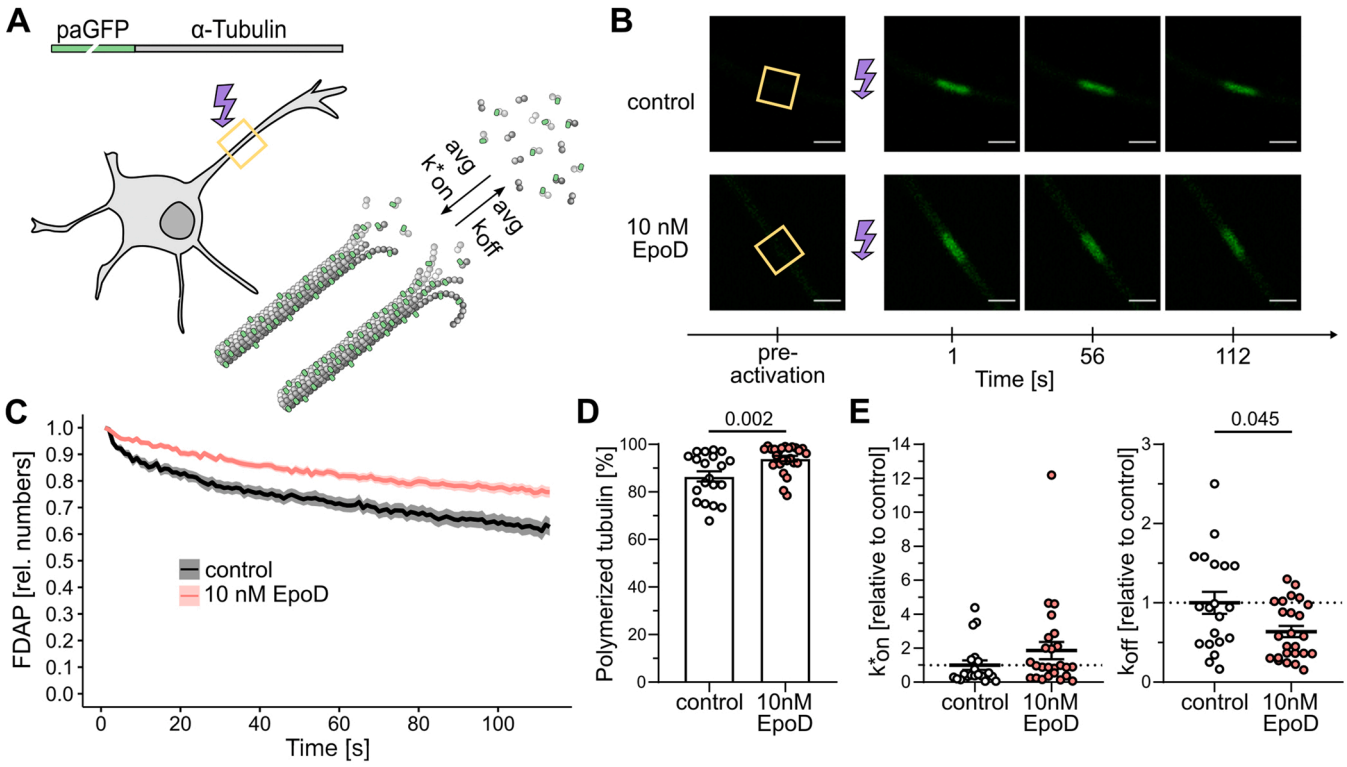

Fig. 1. The microtubule-targeting agent epothilone D (EpoD) increases the amount of microtubule polymer in axon-like processes. A. Schematic representation of the Fluorescence Decay After Photoactivation (FDAP) approach after transfection of paGFP-α-Tubulin to determine average k^*_{on} and k_{off} rate constants of tubulin polymerization. A short segment in the middle of a process (yellow box) was photoactivated, and the fluorescence decay with time was monitored within this region. B. Representative time-lapse micrographs of FDAP in the absence (top) or presence (bottom) of 10 nM EpoD at the indicated times. Scale bar, 5 μm. C. FDAP diagrams of paGFP-α-Tubulin expressing cells. Mean ± SEM of control cells (black, n = 20) and EpoD-treated cells (red, n = 25) are shown. D. Bar graph of the amount of polymerized tubulin. Mean ± SEM of the experiments in (C) are presented. E. Scatterplots of the association (k^*_{on}) and dissociation rate constants (k_{off}) of the experiments in (C) are shown. Statistically significant differences between samples were determined by an unpaired Student's t-test. P values are shown in the graph.

10 nm and axially below 50 nm (Jungmann et al., 2010). Our samples reached a localization precision of 6.0 ± 0.4 nm for PC12 cells and 6.7 ± 0.2 nm for primary neurons (mean±SEM). The analysis and quantification of the rendered super-resolved z-stacks was performed using the open-source software package SIFNE (Zhang et al., 2017). As Zhang et al. developed their tool for 2D datasets only, we created Maximum Intensity Projections (MIPs) from our datasets. Furthermore, we choose optical slices of 150 nm with the highest resolution to avoid distortion caused by overlapping superimposed microtubules from another plane (Fig. 2A, B). TIRF microscopy in the HILO mode visualized the densely packed network of microtubules in the shaft of axon-like processes of PC12 cells, and downstream analysis with SIFNE enabled the identification of individual microtubules and their intersections (Fig. 2C).

3.3. Quantitative analysis of microtubule arrays reveals that EpoD induces higher microtubule density and reduced mean length of microtubules in axon-like processes

Extraction of the filamentous network of microtubules from cells exposed to 10 nM EpoD revealed a significantly higher density of microtubules, consistent with the FDAP measurements of ensemble microtubule dynamics after microtubule stabilization by EpoD (Fig. 3A). In addition to an increased amount of microtubule polymer, the structure of the microtubules was altered in terms of their straightness, which was determined from the end-to-end distance of individual filaments, and the density of intersections where closely spaced microtubules crossed each other (Fig. 3B, C). Interestingly, EpoD induced a shift in microtubule length distribution towards shorter ones (Fig. 3D, E). This resulted in a significant decrease in mean microtubule lengths from 2.39 μm to 1.98 μm. Thus, the data indicate that the super-resolution approach using DNA-PAINT followed by algorithm-based image analysis enables the determination of microtubule organization in axon-like processes of model neurons with incorporated mEGFP-tagged tubulin. They also provide evidence that the MTA EpoD induces specific changes in the organization of the microtubule array in terms of the length of the individual microtubules, their straightness, and their overall density.

3.4. Super-resolution imaging of microtubule arrays in dendrites of cultured hippocampal neurons

For comparison with the axon-like microtubule array, we also determined the organization of microtubules in dendrites of cultured hippocampal neurons, where the axial spacing between microtubules is very similar (Chen et al., 1992; Jacobs and Stevens, 1986). The analysis of axonal microtubule organization involved prior transfection with mEGFP-tagged tubulin to allow direct detection of the microtubules with a nanobody targeting GFP. While such an approach can be easily implemented in cell lines, it is more challenging to perform in primary neurons, which are generally more difficult to transfect and much more sensitive to manipulation.

Therefore, we employed a different labeling strategy using an anti-α-tubulin polyclonal antibody and an oligonucleotide-labeled nanobody against the tubulin antibody light chain. In addition, in order to visualize and select proper neurons to be imaged with DNA-PAINT, immunostaining was performed using an anti-β-tubulin monoclonal antibody and anti-mouse Alexa Fluor® 488 as a secondary antibody. We applied this labeling strategy to primary hippocampal neurons and imaged their dendrites by TIRF super-resolution microscopy in the HILO mode with DNA-PAINT. The spacing between individual microtubules in dendrites (64 ± 10 nm) is known to be slightly smaller than in PC12 (70 ± 20 nm)

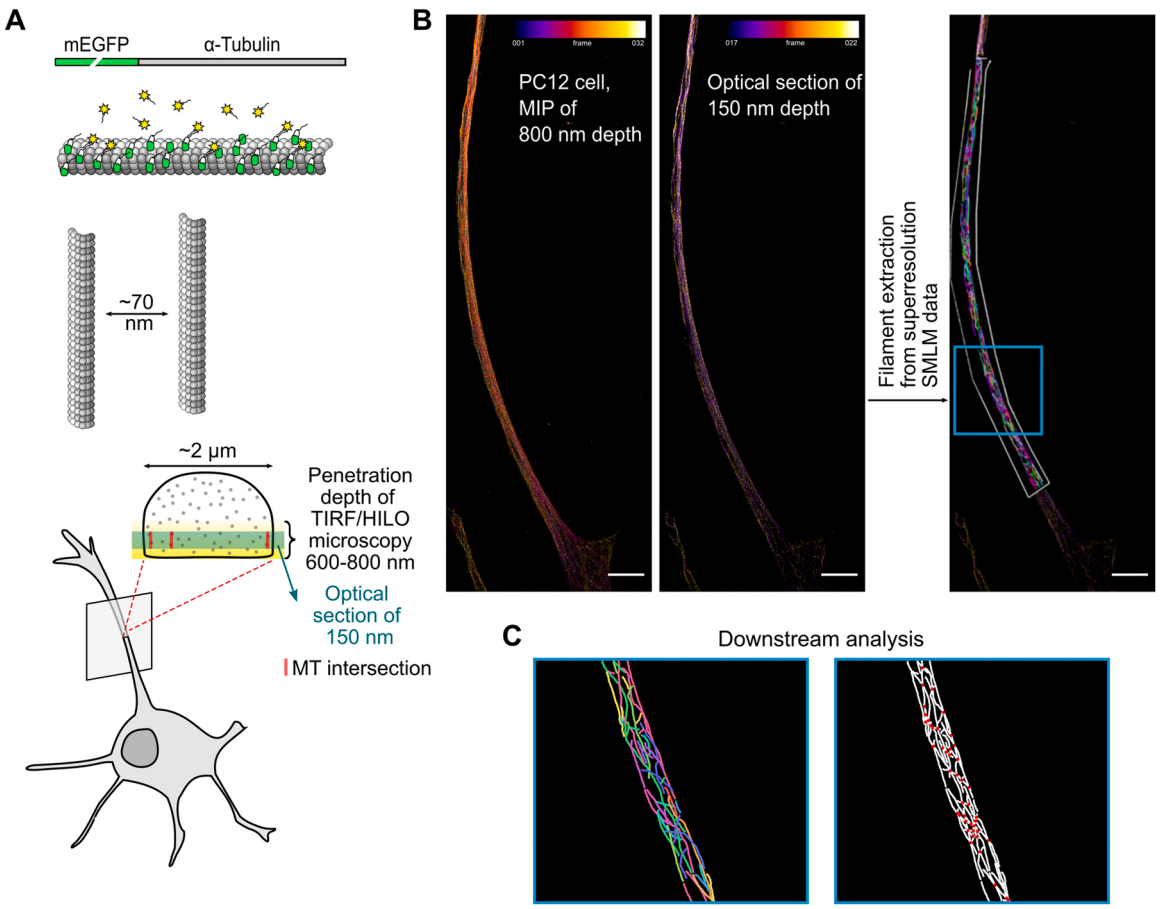

Fig. 2. : Super-resolution imaging of microtubule arrays in axon-like processes. A. Schematic representation of the super-resolution imaging approach with DNA-PAINT to visualize microtubule organization in axon-like processes of PC12 cells. Cells were transfected with mEGFP-α-Tubulin and the transient hybridization between oligonucleotide strands tagged to nanobodies against GFP and free diffusing dye-labeled (Cy3B) oligonucleotide strands was visualized. B. Maximum Intensity Projection (MIP) of 3D rendered single-molecule localization (SML) data represented with a fire color code is shown. Scale bar, 5 µm. An optical section of 150 nm thickness from the SML data with the best resolution is shown to the right. A selected ROI was processed with SIFNE to trace individual microtubules overlaid with a rainbow color code in the micrograph. C. Enlarged representations of the detected microtubule filaments (rainbow color code) and their intersections (red dots) from the downstream analysis are shown.

as determined by previous electron microscopic analyses (Chen et al., 1992; Jacobs and Stevens, 1986). Therefore, we essentially followed the same approach as for PC12 cells in terms of creating MIPs from optical sections but reduced their thickness to 100 nm to account for the reduced spacing (Fig. 4A, B). The distribution of microtubules appeared to be very similar in the dendrites compared to axon-like processes.

3.5. Quantitative analysis of dendritic microtubule arrays shows organization similar to that of microtubules in axon-like processes

Quantitative analysis of the dendritic microtubule array was performed using the same approach as for the microtubules in axon-like processes. Quantification of microtubule density and length distribution yielded very similar numbers for hippocampal neurons and model neurons (Fig. 5A, D, E). The straightness of the microtubules and the frequency of microtubule intersections were also very similar (Fig. 5B, C). Thus, the data indicate that the super-resolution approach with DNA-PAINT followed by algorithm-based image analysis allows to quantify the organization of microtubules also in dendrites of primary neurons. In addition, the data indicate that the properties of the microtubule arrays in axon-like processes of model neurons and dendrites of hippocampal neurons are surprisingly similar.

4. Discussion

Electron microscopy (EM) has long been the gold standard for determining the organization of the cytoskeleton in neuronal processes. Since the beautiful pictures by Nobutuka Hirokawa and others in the early 1980s (Hirokawa, 1982; Hirokawa et al., 1985, 1984), major strides have been made to make this time-consuming and labor-intensive imaging strategy more efficient through the development of high-throughput EM approaches (Yin et al., 2020). Nowadays, alternative imaging strategies such as SMLM using nanobodies are able to resolve bundled microtubules in neurons (Mikhaylova et al., 2015) and other super-resolution approaches allow new insights into the organization of brain cells during physiology and disease (Choquet et al., 2021; Padmanabhan et al., 2021). However, the automated extraction of tangled filamentous structures has long been the bottleneck in the analysis and quantification of the image data obtained. Several computational approaches have recently emerged that facilitate the reconstruction of these complex networks (Alioscha-Perez et al., 2016; Faulkner et al., 2017; Xia et al., 2019).

We combined super-resolution microscopy by DNA-PAINT, which enabled us to resolve the microtubule lattice in axon-like processes of model neurons and dendrites of primary neurons in 3D, with a computational quantitative analysis of the complex microtubule network based on the software tool SIFNE (Zhang et al., 2017). We determined the microtubule organization regarding microtubule length distribution,

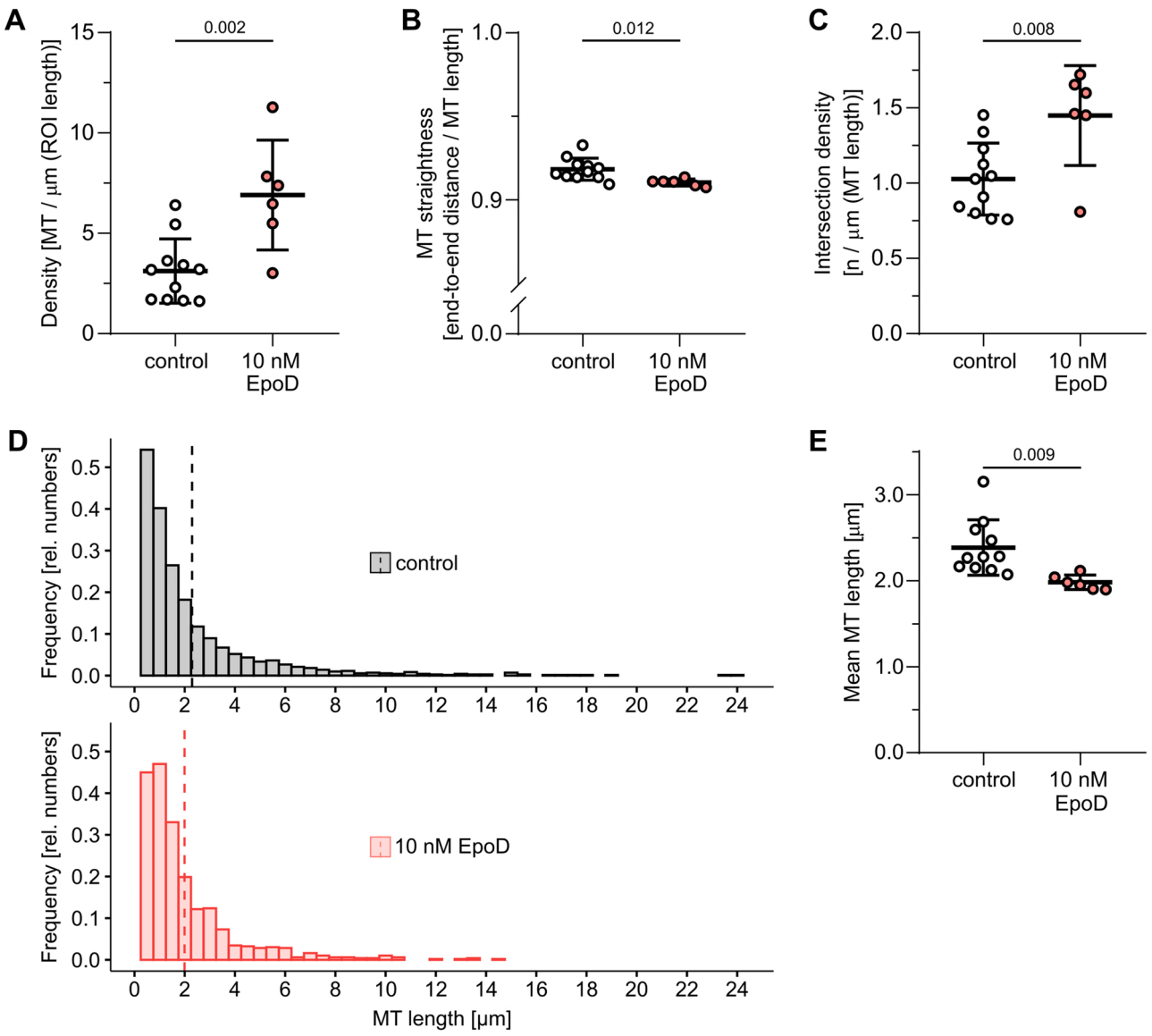

Fig. 3. : Quantitative analysis of microtubule arrays reveals that EpoD induces higher microtubule density and reduced mean length of microtubules in axon-like processes. A-C. Scatterplots showing microtubule density per µm (A), the microtubule straightness (B), and microtubule intersection density (C) in axon-like processes. Scatterplots show means ± SEM from means per cell (control, n = 11 cells; EpoD treatment, n = 6 cells). D. Distribution of microtubule lengths in a relative frequency histogram plot (control, n = 236 from 11 cells; EpoD treatment, n = 307 from 6 cells). Dotted lines indicate the mean microtubule lengths per condition. E. Scatterplot showing the mean microtubule lengths per cell. Statistically significant differences between samples were determined by an unpaired Student's t test. P values are shown in the graph.

density, and mass. In addition, we quantified the straightness of the microtubules and intersections between individual microtubule filaments. Significant changes upon microtubule stabilization by EpoD treatment in the microtubule array in terms of the length of the individual microtubules, their straightness, polymer density, and mass were observed, affecting the frequency of crossing filaments. Changes in microtubule mass and density were consistent with measurements of ensemble microtubule dynamics in live cells by FDAP. In addition, we demonstrate the robustness of the imaging and quantification strategy with respect to the labeling of microtubule filaments, neuronal cell types, and neurites. Our results are consistent with data obtained by serial reconstruction from EM images or by tracing microtubule filaments after microinjection of biotin-labeled tubulin (Wang et al., 1996; Yu and Baas, 1994). While it would be interesting to perform a similar analysis in axons of primary neurons, it should be noted that while the microtubule spacing is relatively high (~70 nm) in axon-like processes of PC12 cells, it is much narrower in the axons of primary neurons, where a spacing of less than 50 nm (stage 4 axons) or even about 10 nm (early stage 3 axons) has been observed in electron microscopic studies of cultured hippocampal neurons (Yu and Baas, 1994). Therefore, especially after treatment with EpoD, the microtubule distance can easily fall below the resolution limit of our quantification strategy, which can affect the accuracy of the analysis and needs further refinement.

It is known that microtubule-stabilizing agents, such as EpoD, stabilize microtubules and perturb their growth by repressing their dynamic instability in a dose-dependent manner (Derry et al., 1995; Rai et al., 2020; Schiff et al., 1979). Short microtubules within neurites act as microtubule nucleation sites (Baas et al., 2016). *In vitro* studies showed that microtubule nucleation sites are stabilized by MTAs and as the concentration of the stabilizer increases, the critical concentration of tubulin required for polymerization decreases (Verma et al., 2016). Since fewer tubulin molecules are available for growth as they are incorporated into many short microtubules, the microtubules become

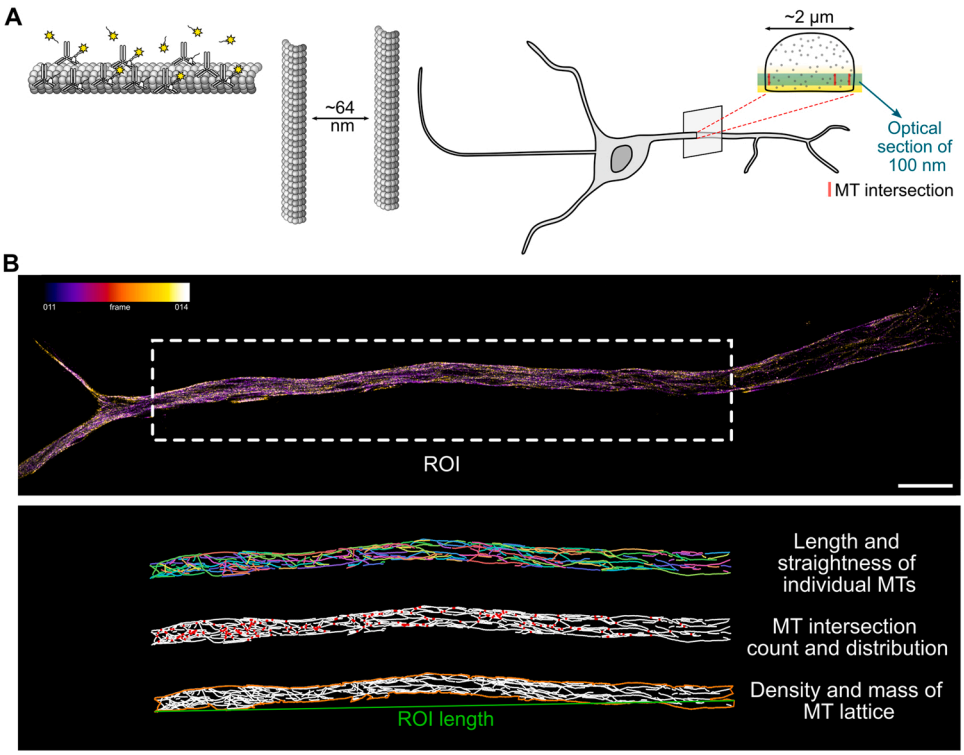

Fig. 4. : Super-resolution imaging of microtubule arrays in dendrites of cultured hippocampal neurons. A. Schematic representation of the super-resolution imaging approach with DNA-PAINT to quantify microtubule organization in dendrites of primary neurons. Cells were immunostained using anti-α-tubulin monoclonal antibody and an oligonucleotide-labeled nanobody against the tubulin antibody light chain. Visualization was performed using free diffusing dye-labeled oligonucleotide strands. B. Maximum Intensity Projection (MIP) of 3D-rendered single-molecule localization (SML) data from an optical section of 100 nm thickness of a hippocampal dendrite represented with a fire color code is shown. Scale bar, 5 µm. The selected ROI was processed with SIFNE to trace individual microtubules, overlaid with a rainbow color code in the micrograph. Extracted filaments with intersections (red dots) are shown below. Density and mass were referred to the length of the analyzed region as indicated at the bottom.

shorter on average even though the total amount of polymer is increased. We have previously found a similar effect of MAPs in cell-free assembly reactions, where higher concentrations of tau resulted in more but shorter microtubules (Brandt and Lee, 1993). With purified components, MTAs mainly reduced the dissociation rate constant at both microtubule ends while having little effect on the association rate (Wilson et al., 1985). Our live cell FDAP measurements after microtubule stabilization in axon-like processes reflect the observations from the in vitro studies showing that the k_{off} rate constant is significantly reduced after substoichiometric EpoD treatment, while the k_{on} rate constant is less affected (see Fig. 1E). Quantification of microtubules based on our super-resolution microscopy data revealed the impact of microtubule stabilization on microtubule length in a cellular setting. Consistent with the in vitro data, we observed a much higher microtubule density but a significantly shorter mean microtubule length (Fig. 3A, E). Such a shift in microtubule array property may explain the negative effect of EpoD on microtubule-based axonal transport as we previously reported in the same cell system (Conze et al., 2022). Molecular motor proteins use the microtubules as tracks for the transport of vesicles and organelles, and the length of the cargo run correlates with the length of the individual microtubules. The motors pause when encountering microtubule-termini before changing tracks and proceeding with cargo transport, suggesting that switching microtubule tracks is limiting for efficient transport (Yogev et al., 2016).

SIFNE uses Line Filter Transform (LFT) and Orientation Filter Transform (OFT) as enhancement and filtering methods that denoise the image and enhance filamentous features. This enables segmentation and the robust detection of filament tracks by binary segmentation. Although microtubules are relatively parallel in neurites, they pass through numerous intersections. Therefore, for mapping the cytoskeletal network, it is necessary to assign filament identity at each intersection. Zhang et al. (2017) treated each detected filament track between intersections as a fragment and used an algorithm to assign filament identity before and after each intersection. The assignment of filament identity or grouping of filament tracks is based on the incorporation of intrinsic mechanical properties of microtubules as geometric constraints such as propagation and distance vectors of the filament fragments. In areas of low microtubule abundance or very high parallelism where no intersection sites are present, filament tracks cannot be grouped simply because additional filament fractions are not present (Fig. S1A). SIFNE provides the ability to exclude ungrouped filaments to avoid bias in densely packed and complex regions where ungrouped filament fragments could skew the analysis. However, in regions of neurites where microtubules are highly parallel or low in number, this strategy leads to a bias in the analysis since a considerable number of filaments would be excluded. We compared our datasets regarding the inclusion or exclusion of these grouped and ungrouped filaments and found a significant effect on mean filament length (Fig. S1B). Therefore, we included all detected filaments in our analysis and set a general cut-off for very short filaments below 375 nm to account for microscopic noise. The number of identified microtubules also affects the number of intersections and density found in neurites, although the differences did not reach significance. We further compared different neurites of individual cells to assess whether the region of interest (ROI) specified by the experimenter affects the overall outcome of the analysis (Fig. S1C). As shown in Fig. S1D, we found no difference when comparing individual ROIs of cells to the overall means per cell examined.

Although our image acquisition allowed us to obtain 3D data, this information was not fully exploited as we overlaid thin optical slices of neurites to create MIPs. Therefore, setting up protocols to decode the microtubule lattice in 3D may provide a further improvement of the approach, which will be useful to analyze the structure of the microtubule array in axons of primary neurons, where the microtubule spacing is much closer (Yu and Baas, 1994).

CRediT authorship contribution statement

Christian Conze: Investigation; Methodology; Writing - original draft. **Nataliya I. Trushina**: Investigation; Data curation; Visualization; Writing - review & editing. **Michael Holtmannspötter**: Methodology; Software; Writing - review & editing. **Marina Rierola**: Investigation; Methodology; Writing - review & editing. **Simone Attanasio**:

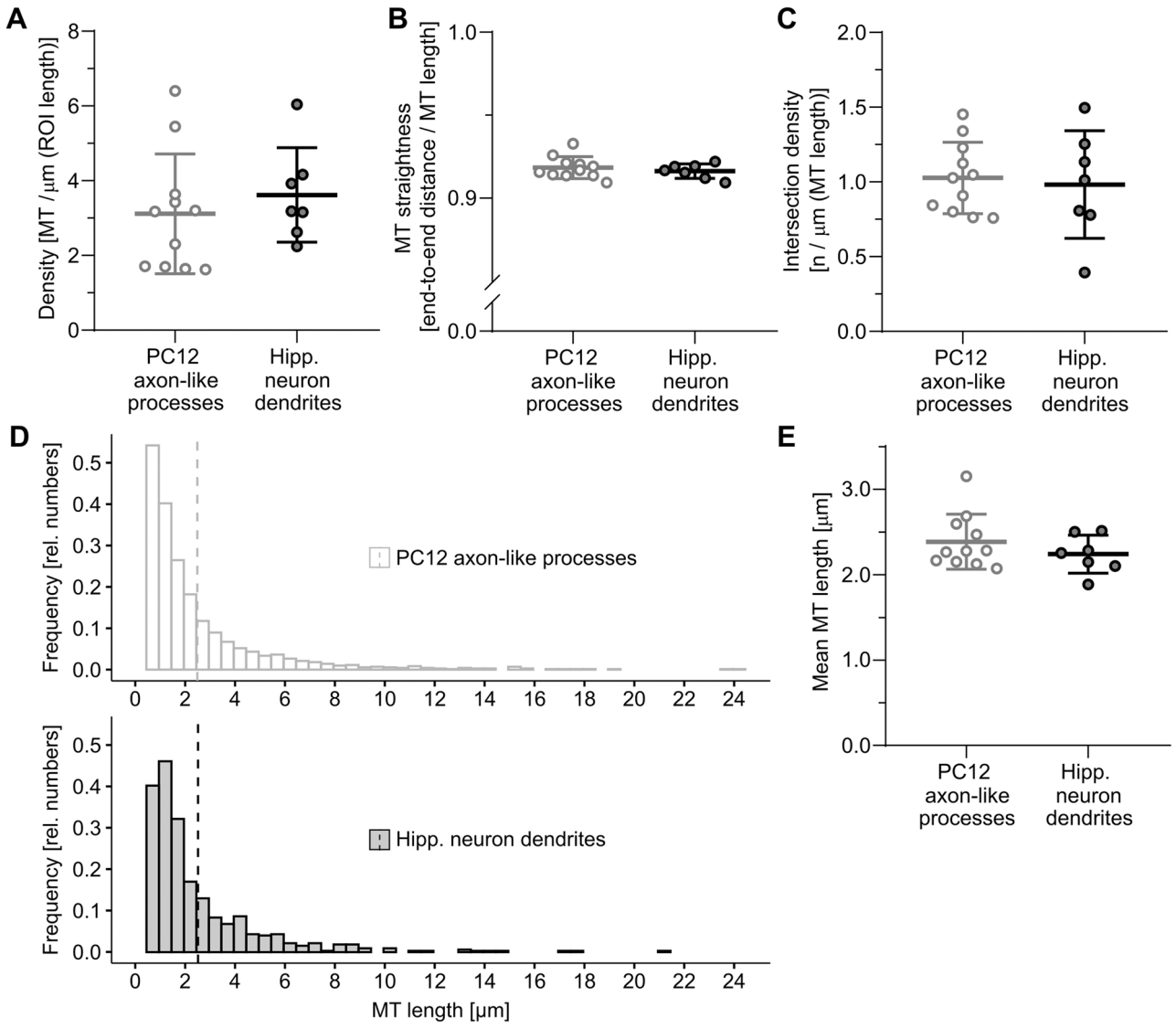

Fig. 5. : Quantitative analysis of dendritic microtubule arrays shows organization similar to that of microtubules in axon-like processes. A-C. Scatterplots showing microtubule density per µm (A), microtubule straightness (B), and microtubule intersection density (C) in dendrites. The scatterplots show the mean ± SEM from the means per cell (n = 7 cells). For comparison, the respective results of axon-like processes, as determined in Fig. 3A-C, are shown in gray. D. Distribution of microtubule lengths in a relative frequency histogram plot (n = 190 from 7 cells). The dotted line indicates the mean microtubule length. For comparison, the mean microtubule length from axon-like processes, as determined in Fig. 3D, is shown in gray. E. Scatterplot showing the mean microtubule lengths per cell. For comparison, the respective results of axon-like processes, as determined in Fig. 3E, is shown in gray.

Investigation; Writing - review & editing. **Lidia Bakota**: Methodology; Supervision; Writing - review & editing. **Jacob Piehler**: Funding acquisition; Resources; Supervision; Writing - review & editing. **Roland Brandt**: Conceptualization; Funding acquisition; Project administration; Supervision; Writing - original draft; Writing - review & editing.

Data availability

Data will be made available on request.

Acknowledgment

This work was supported by the Deutsche Forschungsgemeinschaft (SFB 944 project Z, no. 180879236 and the DFG Facility iBiOs, no. 324775161 to JP, DFG BR1192/14–1 to RB) and European Union's Horizon 2020 research and innovation program H2020-MSCAITN-2019-EJD - Grant agreement no: 860070 (SA and RB).

Appendix A. Supporting information

Supplementary data associated with this article can be found in the online version at doi:10.1016/j.brainresbull.2022.10.008.

References

Agasti, S.S., Wang, Y., Schueder, F., Sukumar, A., Jungmann, R., Yin, P., 2017. DNA-barcoded labeling probes for highly multiplexed Exchange-PAINT imaging. Chem. Sci. 8, 3080–3091.

Akhmanova, A., Steinmetz, M.O., 2015. Control of microtubule organization and dynamics: two ends in the limelight. Nat. Rev. Mol. Cell Biol. 16, 711–726.

Alioscha-Perez, M., Benadiba, C., Goossens, K., Kasas, S., Dietler, G., Willaert, R., Sahli, H., 2016. A robust actin filaments image analysis framework. PLOS Comput. Biol. 12, e1005063.

Baas, P.W., Rao, A.N., Matamoros, A.J., Leo, L., 2016. Stability properties of neuronal microtubules. Cytoskeleton 73, 442–460.

Balint, S., Verdeny Vilanova, I., Sandoval Alvarez, A., Lakadamyali, M., 2013. Correlative live-cell and superresolution microscopy reveals cargo transport dynamics at microtubule intersections. Proc. Natl. Acad. Sci. USA 110, 3375–3380.

Brandt, R., Bakota, L., 2017. Microtubule dynamics and the neurodegenerative triad of Alzheimer's disease: the hidden connection. J. Neurochem. 143, 409–417.
Brandt, R., Lee, G., 1993. The balance between tau protein's microtubule growth and nucleation activities: implications for the formation of axonal microtubules. J. Neurochem. 61, 997–1005.
Brandt, R., Leger, J., Lee, G., 1995. Interaction of tau with the neural plasma membrane mediated by tau's amino-terminal projection domain. J. Cell Biol. 131, 1327–1340.
Brandt, R., Trushina, N.I., Bakota, L., 2020. Much more than a cytoskeletal protein: physiological and pathological functions of the non-microtubule binding region of Tau. Front. Neurol. 11, 590059.
Bray, D., Bunge, M.B., 1981. Serial analysis of microtubules in cultured rat sensory axons. J. Neurocytol. 10, 589–605.
Buey, R.M., Diaz, J.F., Andreu, J.M., O'Brate, A., Giannakakou, P., Nicolaou, K.C., Sasmal, P.K., Ritzen, A., Namoto, K., 2004. Interaction of epothilone analogs with the paclitaxel binding site: relationship between binding affinity, microtubule stabilization, and cytotoxicity. Chem. Biol. 11, 225–236.
Chalfie, M., Thomson, J.N., 1979. Organization of neuronal microtubules in the nematode Caenorhabditis elegans. J. Cell Biol. 82, 278–289.
Chen, J., Kanai, Y., Cowan, N.J., Hirokawa, N., 1992. Projection domains of MAP2 and tau determine spacings between microtubules in dendrites and axons. Nature 360, 674–677.
Choquet, D., Sainlos, M., Sibarita, J.B., 2021. Advanced imaging and labelling methods to decipher brain cell organization and function. Nat. Rev. Neurosci. 22, 237–255.
Conze, C., Rierola, M., Trushina, N.I., Peters, M., Janning, D., Holzer, M., Heinisch, J.J., Arendt, T., Bakota, L., Brandt, R., 2022. Caspase-cleaved tau is senescence-associated and induces a toxic gain of function by putting a brake on axonal transport. Mol. Psychiatry 27, 3010–3023.
Derry, W.B., Wilson, L., Jordan, M.A., 1995. Substoichiometric binding of taxol suppresses microtubule dynamics. Biochemistry 34, 2203–2211.
Dubey, J., Ratnakaran, N., Koushika, S.P., 2015. Neurodegeneration and microtubule dynamics: death by a thousand cuts. Front. Cell Neurosci. 9, 343.
Fath, T., Eidenmüller, J., Brandt, R., 2002. Tau-mediated cytotoxicity in a pseudohyperphosphorylation model of Alzheimer's disease. J. Neurosci. 22, 9733.
Fath, T., Ke, Y.D., Gunning, P., Gotz, J., Ittner, L.M., 2009. Primary support cultures of hippocampal and substantia nigra neurons. Nat. Protoc. 4, 78–85.
Faulkner, C., Zhou, J., Evrard, A., Bourdais, G., MacLean, D., Haweker, H., Eckes, P., Robatzek, S., 2017. An automated quantitative image analysis tool for the identification of microtubule patterns in plants. Traffic 18, 683–693.
Hirokawa, N., 1982. Cross-linker system between neurofilaments, microtubules, and membranous organelles in frog axons revealed by the quick-freeze, deep-etching method. J. Cell Biol. 94, 129–142.
Hirokawa, N., Glicksman, M.A., Willard, M.B., 1984. Organization of mammalian neurofilament polypeptides within the neuronal cytoskeleton. J. Cell Biol. 98, 1523–1536.
Hirokawa, N., Bloom, G.S., Vallee, R.B., 1985. Cytoskeletal architecture and immunocytochemical localization of microtubule-associated proteins in regions of axons associated with rapid axonal transport: the beta,beta'-iminodipropionitrile-intoxicated axon as a model system. J. Cell Biol. 101, 227–239.
Igaev, M., Janning, D., Sundermann, F., Niewidok, B., Brandt, R., Junge, W., 2014. A refined reaction-diffusion model of tau-microtubule dynamics and its application in FDAP analysis. Biophys. J. 107, 2567–2578.
Jacobs, J.R., Stevens, J.K., 1986. Changes in the organization of the neuritic cytoskeleton during nerve growth factor-activated differentiation of PC12 cells: a serial electron microscopic study of the development and control of neurite shape. J. Cell Biol. 103, 895–906.
Janning, D., Igaev, M., Sundermann, F., Bruhmann, J., Beutel, O., Heinisch, J.J., Bakota, L., Piehler, J., Junge, W., Brandt, R., 2014. Single-molecule tracking of tau reveals fast kiss-and-hop interaction with microtubules in living neurons. Mol. Biol. Cell 25, 3541–3551.
Joshi, H.C., Baas, P., Chu, D.T., Heidemann, S.R., 1986. The cytoskeleton of neurites after microtubule depolymerization. Exp. Cell Res. 163, 233–245.
Jungmann, R., Steinhauer, C., Scheible, M., Kuzyk, A., Tinnefeld, P., Simmel, F.C., 2010. Single-molecule kinetics and super-resolution microscopy by fluorescence imaging of transient binding on DNA origami. Nano Lett. 10, 4756–4761.
Kapitein, L.C., Hoogenraad, C.C., 2015. Building the neuronal microtubule cytoskeleton. Neuron 87, 492–506.
Lee, C.B., Wu, Z., Zhang, F., Chappell, M.D., Stachel, S.J., Chou, T.C., Guan, Y., Danishefsky, S.J., 2001. Insights into long-range structural effects on the stereochemistry of aldol condensations: a practical total synthesis of desoxyepothilone F. J. Am. Chem. Soc. 123, 5249–5259.
Lee, G., Rook, S.L., 1992. Expression of tau protein in non-neuronal cells: microtubule binding and stabilization. J. Cell Sci. 102 (Pt 2), 227–237.
Letourneau, P.C., 1982. Analysis of microtubule number and length in cytoskeletons of cultured chick sensory neurons. J. Neurosci.: Off. J. Soc. Neurosci. 2, 806–814.
Maday, S., Twelvetrees, A.E., Moughamian, A.J., Holzbaur, E.L., 2014. Axonal transport: cargo-specific mechanisms of motility and regulation. Neuron 84, 292–309.
McNally, F.J., Roll-Mecak, A., 2018. Microtubule-severing enzymes: from cellular functions to molecular mechanism. J. Cell Biol. 217, 4057–4069.
Mikhaylova, M., Cloin, B.M., Finan, K., van den Berg, R., Teeuw, J., Kijanka, M.M., Sokolowski, M., Katrukha, E.A., Maidorn, M., Opazo, F., et al., 2015. Resolving bundled microtubules using anti-tubulin nanobodies. Nat. Commun. 6, 7933.
Millecamps, S., Julien, J.P., 2013. Axonal transport deficits and neurodegenerative diseases. Nat. Rev. Neurosci. 14, 161–176.
Niewidok, B., Igaev, M., Sundermann, F., Janning, D., Bakota, L., Brandt, R., 2016. Presence of a carboxy-terminal pseudorepeat and disease-like pseudohyperphosphorylation critically influence tau's interaction with microtubules in axon-like processes. Mol. Biol. Cell 27, 3537–3549.
Nishida, T., Yoshimura, R., Nishi, R., Imoto, Y., Endo, Y., 2020. Application of ultra-high voltage electron microscope tomography to 3D imaging of microtubules in neurites of cultured PC12 cells. J. Microsc. 278, 42–48.
Okabe, S., Hirokawa, N., 1988. Microtubule dynamics in nerve cells: analysis using microinjection of biotinylated tubulin into PC12 cells. J. Cell Biol. 107, 651–664.
Ovesny, M., Krizek, P., Borkovec, J., Svindrych, Z., Hagen, G.M., 2014. ThunderSTORM: a comprehensive ImageJ plug-in for PALM and STORM data analysis and super-resolution imaging. Bioinformatics 30, 2389–2390.
Padmanabhan, P., Kneynsberg, A., Gotz, J., 2021. Super-resolution microscopy: a closer look at synaptic dysfunction in Alzheimer disease. Nat. Rev. Neurosci. 22, 723–740.
Penazzi, L., Bakota, L., Brandt, R., 2016a. Microtubule dynamics in neuronal development, plasticity, and neurodegeneration. Int. Rev. Cell Mol. Biol. 321, 89–169.
Penazzi, L., Tackenberg, C., Ghori, A., Golovyashkina, N., Niewidok, B., Selle, K., Ballatore, C., Smith 3rd, A.B., Bakota, L., Brandt, R., 2016b. Abeta-mediated spine changes in the hippocampus are microtubule-dependent and can be reversed by a subnanomolar concentration of the microtubule-stabilizing agent epothilone D. Neuropharmacology 105, 84–95.
Prokop, A., 2020. Cytoskeletal organization of axons in vertebrates and invertebrates. J. Cell Biol. 219.
Rai, A., Liu, T., Glauser, S., Katrukha, E.A., Estevez-Gallego, J., Rodriguez-Garcia, R., Fang, W.S., Diaz, J.F., Steinmetz, M.O., Altmann, K.H., et al., 2020. Taxanes convert regions of perturbed microtubule growth into rescue sites. Nat. Mater. 19, 355–365.
Rivkin, A., Yoshimura, F., Gabarda, A.E., Cho, Y.S., Chou, T.C., Dong, H., Danishefsky, S. J., 2004. Discovery of (*E*)-9,10-dehydroepothilones through chemical synthesis: on the emergence of 26-trifluoro-(*E*)-9,10-dehydro-12,13-desoxyepothilone B as a promising anticancer drug candidate. J. Am. Chem. Soc. 126, 10913–10922.
Ruschel, J., Hellal, F., Flynn, K.C., Dupraz, S., Elliott, D.A., Tedeschi, A., Bates, M., Sliwinski, C., Brook, G., Dobrindt, K., et al., 2015. Axonal regeneration. Systemic administration of epothilone B promotes axon regeneration after spinal cord injury. Science 348, 347–352.
Schiff, P.B., Fant, J., Horwitz, S.B., 1979. Promotion of microtubule assembly in vitro by taxol. Nature 277, 665–667.
Schnitzbauer, J., Strauss, M.T., Schlichthaerle, T., Schueder, F., Jungmann, R., 2017. Super-resolution microscopy with DNA-PAINT. Nat. Protoc. 12, 1198–1228.
Soliman, A., Bakota, L., Brandt, R., 2022. Microtubule-modulating agents in the fight against neurodegeneration: will it ever work? Curr. Neuropharmacol. 20, 782–798.
Tian, N., Hanson, K.A., Canty, A.J., Vickers, J.C., King, A.E., 2020. Microtubule-dependent processes precede pathological calcium influx in excitotoxin-induced axon degeneration. J. Neurochem. 152, 542–555.
Tokunaga, M., Imamoto, N., Sakata-Sogawa, K., 2008. Highly inclined thin illumination enables clear single-molecule imaging in cells. Nat. Methods 5, 159–161.
Verma, S., Kumar, N., Verma, V., 2016. Role of paclitaxel on critical nucleation concentration of tubulin and its effects thereof. Biochem. Biophys. Res. Commun. 478, 1350–1354.
Wang, J., Yu, W., Baas, P.W., Black, M.M., 1996. Microtubule assembly in growing dendrites. J. Neurosci.: Off. J. Soc. Neurosci. 16, 6065–6078.
Weiss, P.A., Mayr, R., 1971. Organelles in neuroplasmic ("axonal") flow: neurofilaments. Proc. Natl. Acad. Sci. USA 68, 846–850.
Wilson, C., Gonzalez-Billault, C., 2015. Regulation of cytoskeletal dynamics by redox signaling and oxidative stress: implications for neuronal development and trafficking. Front. Cell. Neurosci. 9, 381.
Wilson, L., Miller, H.P., Farrell, K.W., Snyder, K.B., Thompson, W.C., Purich, D.L., 1985. Taxol stabilization of microtubules in vitro: dynamics of tubulin addition and loss at opposite microtubule ends. Biochemistry 24, 5254–5262.
Xia, S., Lim, Y.B., Zhang, Z., Wang, Y., Zhang, S., Lim, C.T., Yim, E.K.F., Kanchanawong, P., 2019. Nanoscale architecture of the cortical actin cytoskeleton in embryonic stem cells. Cell Rep. 28 (1251–1267), e1257.
Yin, W., Brittain, D., Borseth, J., Scott, M.E., Williams, D., Perkins, J., Own, C.S., Murfitt, M., Torres, R.M., Kapner, D., et al., 2020. A petascale automated imaging pipeline for mapping neuronal circuits with high-throughput transmission electron microscopy. Nat. Commun. 11, 4949.
Yogev, S., Cooper, R., Fetter, R., Horowitz, M., Shen, K., 2016. Microtubule organization determines axonal transport dynamics. Neuron 92, 449–460.
Yu, W., Baas, P.W., 1994. Changes in microtubule number and length during axon differentiation. J. Neurosci.: Off. J. Soc. Neurosci. 14, 2818–2829.
Zhang, Z., Nishimura, Y., Kanchanawong, P., 2017. Extracting microtubule networks from superresolution single-molecule localization microscopy data. Mol. Biol. Cell 28, 333–345.